Mathematical modelling to support traceable dynamic calibration of pressure sensors

C Matthews[1], F Pennecchi[2], S Eichstädt[3], A Malengo[2], T Esward[1], I Smith[1], C Elster[3], A Knott[1], F Arrhén[4], A Lakka[5]

[1]National Physical Laboratory, United Kingdom
[2]Istituto Nazionale di Ricerca Metrologica, Italy
[3]Physikalisch-Technische Bundesanstalt, Germany
[4]SP Sveriges Tekniska Forskningsinstitut, Sweden
[5]Mittatekniikan Keskus, Finland

E-mail: clare.matthews@npl.co.uk

Abstract.

This paper focuses on the mathematical modelling required to support the development of new primary standard systems for traceable calibration of dynamic pressure sensors. We address two fundamentally different approaches to realising primary standards, specifically the shock tube method and the drop-weight method. Focusing on the shock tube method, the paper presents first results of system identification and discusses future experimental work that is required to improve the mathematical and statistical models.

We use simulations to identify differences between the shock tube and drop-weight methods, to investigate sources of uncertainty in the system identification process and to assist experimentalists in designing the required measuring systems. We demonstrate the identification method on experimental results and draw conclusions.

Keywords Traceability, dynamic measurement, pressure sensor calibration, shock tube, drop-weight system

1. Introduction

At present traceability exists for static realisations of the mechanical quantities force, torque and pressure. This traceability is established through validated primary calibration systems together with a standardised uncertainty evaluation in line with the *Guide to the expression of uncertainty in measurement* (GUM) and related documents [1, 2, 3]. The European Metrology Research Programme (EMRP) project IND09 *Traceable Dynamic Measurement of Mechanical Quantities* is designed to address the extension of traceability to dynamic measurements of these quantities, i.e., to those cases in which the frequency-dependent response of a sensor cannot be described by a single parameter (sensitivity) from static calibration. In these cases there is a need to correct the measured data for the bandwidth-limitations of the sensor. This

correction requires that a dynamic model for the sensor be established through a dynamic calibration [4, 5, 6, 7, 8].

Many applications of the measurement of mechanical quantities such as force, torque and pressure are of a dynamic type, i.e., the measurand shows a strong variation over time. The sensors employed in such applications are in most cases calibrated only by purely static procedures owing to a lack of commonly accepted procedures or documentary standards for the dynamic calibration of mechanical sensors, see, e.g., [8, 9, 10, 11, 12] and references therein. On the other hand, it is well known that mechanical sensors exhibit distinctive dynamic behaviour that shows an increasing deviation from their static sensitivity characteristic as the frequency increases. These limitations lead not only to inaccurate measurement results but in some cases can culminate in an almost complete ignorance of the magnitude of the measurement uncertainty; see, for instance, [13] for a comparison of static and dynamic uncertainty evaluation.

To support emerging industrial needs for calibrated pressure sensors for dynamic applications, four European NMIs (SP: Sweden, MIKES: Finland, PTB: Germany, NPL: UK) are developing new primary measurement standards that can generate time-varying pressure signals of the required bandwidth and dynamic range. Two primary standard systems are being developed and compared: shock tubes (NPL, SP) and drop-weight systems (MIKES, PTB). The two techniques cover different pressure and frequency intervals and a key metrology challenge is to establish traceability over as wide pressure and frequency intervals as possible, while ensuring agreement between the two techniques and agreement between dynamic and static pressure calibrations.

New mathematical and statistical techniques are required to underpin the development of these calibration methods, specifically: the development and identification of models of the complete dynamic measurement chain and its constituent parts as, e.g., in [6]; a consistent treatment of uncertainty evaluation and propagation both in NMI-based primary calibration procedures and secondary methods used for industrial applications [7, 8]; and the reconstruction of the input signal by the deconvolution of sensor and system effects from the output signal, to enable reliable evaluation of the dynamic quantity of interest and its associated uncertainty [14, 15].

The goal of this paper is to highlight the mathematical challenges in the development of a primary standard for dynamic pressure calibration and to present new results of system identification. The paper focuses in particular on available approaches to modelling and measuring the input signal and the subsequent identification of the sensor or extended measuring system. In this work we consider calibration of a measuring chain, comprising a sensor and a charge amplifier. Therefore throughout the remainder of this paper, we will use the term *measuring system* to refer to a multi-component measuring chain, and to distinguish between this chain and the sensor component of the chain.

A simulation approach has been used to study and develop the necessary mathematical tools to support the new dynamic pressure calibration methodologies.

There are a number of stages to the calibration process and it is important to understand the effect of each of these stages on the resulting calibration. The pressure signals generated by the shock tube and drop-weight system are very different in terms of magnitude, duration and bandwidth. Simulating the response of a measuring system to these different types of input signals can help to identify the potential scope and capability of the two calibration systems and to establish minimum requirements for the respective input signals to achieve target uncertainties. The final output from the calibration depends on the type of measuring system used, the signal processing techniques applied to process the measurements and the form in which the results are provided. By simulating the full calibration process, it is possible to estimate the effect on uncertainties of applying different analysis techniques and of providing, for example, a calibration in terms of an amplitude and phase frequency response at a given set of frequencies, compared to a full parametric model describing the measuring system response.

The structure of this paper is as follows. In Section 2 we introduce the calibration systems considered, namely shock tubes and drop-weight systems, and identify the pressure and frequency intervals that we expect to achieve with each system. Section 3 details the simulation approach we have taken and demonstrates calibration software that provides a frequency response for a measuring system. In Section 4 the software is extended to fit a parametric model to the measuring system response. Analysis of shock tube data is described in Section 5. Conclusions and an outlook to future work are set out in Section 6.

2. Dynamic calibration of pressure sensors

A calibration process typically requires a known input to be provided to a sensor (or measuring system) and the recording of the response to that known input. For dynamic systems that can be modelled as a linear time-invariant system, the input signal and the output response signal are then employed in a system identification process to derive the transfer function (frequency domain) or impulse response (time domain) of the sensor [4, 5]. This process can be described by

$$y(t) = h(t) * x(t) + \varepsilon(t), \tag{1}$$

where "$*$" denotes convolution, $x(t)$ is the generated time-dependent pressure input signal, $h(t)$ the sensor impulse response, $y(t)$ the output signal, and $\varepsilon(t)$ the measurement noise. A description of the sensor behaviour may be derived in different forms. One form frames the calibration problem as a deconvolution process: assuming the pressure input $x(t)$ is known, the ratio of the Fourier transforms of the output signal and known input signal will estimate the frequency response of the sensor [16]. Alternatively, the problem may be viewed as a system identification task where a parameterised model of the sensor is fitted to a model (1) or the corresponding Fourier ratio, for a known pressure input $x(t)$ [17].

Both methods of analysis assume that the sensor under calibration exhibits linear behaviour. Pressures used to calibrate a sensor should remain well within the limits stated by the manufacturer, to ensure that this assumption remains accurate. It should also be noted that any calibration results, whether a frequency response or a parameterised model, will only be valid up to the maximum pressures used in calibration. No assumption of linearity can be assumed beyond this pressure.

We consider two different systems for the generation of the time-varying pressure input: shock tubes and drop-weight systems. These two systems are described in Sections 2.2 and 2.3, respectively.

2.1. Primary standard systems for dynamic pressure

A primary calibration system is required to allow reliable traceability for the measurement of dynamic pressure. Despite development studies carried out at the National Institute of Standards and Technology (NIST), USA [18, 19], to the authors' knowledge, the use of shock tubes as a primary calibration system has not yet been fully realised. Similarly, to date drop-weight systems have been used only as secondary calibrators. A reference sensor and the sensor to be calibrated are usually compared by means of the drop-weight system, with traceability for the reference sensor being reached by static calibration.

Primary calibration requires independent, traceable knowledge of the input pressure to the sensor. The NIST shock tube proposal suggested the use of laser spectrometry to meet this requirement [18]. For the shock tube systems considered here the input signal (the pressure shock front experienced by the sensor undergoing calibration) cannot be measured independently. To this end, it is intended to predict the nature of the shock front by means of mathematical models derived from shock tube theory (e.g., [20]) and traceable measurements of the shock propagation speed and the initial pressure and temperature (e.g., [21]) (see Section 2.2). For the drop-weight systems considered here, a traceable indirect measurement of the input signal is achieved via two different approaches (see Section 2.3); one based on the acceleration measurement of a falling mass, the other on the refractive index variation of a fluid under pressure. For both shock tube and drop-weight systems, the relation of these indirect measurements to an estimate of the time-varying pressure within the system relies on the validity assumption of a theoretical model. The different approaches to knowledge of the input signal will have consequences for uncertainty analysis.

Details of approaches explored for modelling of the pressure input are given below for both the shock tube and drop-weight system.

2.2. Shock tube as a primary calibration system

A shock tube is set up with low-pressure (driven) and high-pressure (driver) sections of the tube, separated by a diaphragm. Sensors to be calibrated are mounted in the end-wall of the driven section. The diaphragm is burst, typically by increasing pressure

in the driver section, generating a shock wave that travels along the driven section. The shock front is reflected off the end-wall of the driven section, causing a fast-rising step change in the pressure at this point.

NPL is building a shock tube with a maximum pressure capacity of 7 MPa, and SP has a shock tube with maximum capacity of 1 MPa. In an ideal shock tube rise times for the pressure step are considered to be almost instantaneous, of the order of 5 ns. Given the relative response time of sensors, it is difficult to measure the rise time of the step in practice. However, in real shock tubes in which diaphragms do not burst instantaneously or only burst partially, and where pressure differences between the driver and driven sections of the shock tube are of the order of only a few MPa, such shock rise times may not be achievable, with tens of nanoseconds being more likely. Such rise times should allow calibrations in the MHz range.

A key challenge concerning the use of shock tubes as a calibration system will be the consistent evaluation of uncertainties associated with the estimate of the pressure input and uncertainties introduced by the use of a step-like calibration signal.

Many previous studies using shock tube-generated pressure waveforms assume an ideal (or near-ideal) step input, e.g., [19, 21, 22]. Under this assumption, the main parameters of a pressure input model are the rise-time and amplitude of the pressure step. From shock tube theory, the amplitude of the pressure gain (ΔP) as the shock front is reflected off the end-wall can be calculated using the starting pressure (P_1) and temperature (T_1) of the driven gas, and the speed of the shock front (V_s) as it travels along the tube. For example, when air is used in the low pressure end of the tube, the pressure gain is calculated as [23]

$$\Delta P = \frac{7}{3} P_1 \left(M_s^2 - 1\right) \left(\frac{2 + 4M_s^2}{5 + M_s^2}\right), \tag{2}$$

where the shock wave Mach number (M_s) is given by

$$M_s = \left(\frac{V_s}{344.5}\right) \sqrt{\frac{298}{T_1}},$$

for temperature T_1 given in K and speed V_s in $\mathrm{m\,s^{-1}}$. Side-wall mounted sensors provide a means of estimating the shock speed, and therefore the expected pressure step.

Experiments were carried out in a prototype shock tube at NPL, to test the applicability of shock tube theory in predicting pressure gain across the reflected shock [24]. This work found good agreement between the changes in pressure predicted by ideal gas theory and the changes in observed sensor output, for a number of different gases, shock wave velocities, and driven section pressure magnitudes. In each case, the mean calculated sensitivity for the pressure sensor lay close to its reported static sensitivity. For the initial analysis, we therefore consider only the uncertainties associated with the measured parameters of initial pressure, temperature and shock speed, with no uncertainty associated with the validity of model 2.

In practice, there may be numerous sources of non-ideal behaviour in the shock tube. For example, non-instantaneous opening of the diaphragm, reflections of a non-planar shock wave from the tube walls, or boundary-layer effects. The diaphragm burst

mechanism is an obvious non-regularity of the shock tube that cannot be controlled from one firing to the next.

A lattice Boltzmann model [25] was developed to investigate this potential source of non-ideal behaviour [26]. Unlike some more traditional methods for modelling fluid flow, the lattice Boltzmann method is able to model discontinuities, such as shock waves. A 3D model was used to investigate both non-instantaneous opening (allowing for opening times up to 30 ms), and symmetrical and non-symmetrical partial opening (allowing for opening proportions down to 20 %). Driven section lengths from 3 to 12 times the diameter, and starting pressure ratios from 2.5 to 10 were used. Results from the model suggest that many disturbances produced by the diaphragm burst can be eliminated by using a sufficiently long shock tube. Both the proposed NPL and SP shock tubes comfortably meet this length requirement. The required tube length may be dependent on the strength of the shock produced. For example, in [27] it was found that for relatively weak shocks, post-shock oscillations were not eliminated by increasing the tube length (though amplitude of the oscillations could be substantially reduced). Experimental investigations into the effects of non-ideal diaphragm burst were made in the prototype shock tube at NPL [24]. Repeated firings were made with diaphragms of different material; aluminium, brass of varying thickness, and copper. The diaphragms possess very different opening mechanisms. For example, ductile aluminium diaphragms petal out and remain intact, while the copper diaphragms tend to shatter open. Over the post-shock region of interest, the (normalised) outputs from the different diaphragms were very repeatable, suggesting that the shock tube was sufficiently long, and the bursting pressures sufficiently high to overcome any diaphragm effects on the signal. Again, the dimensions and pressure ranges of the proposed NPL and SP shock tubes exceed those of the prototype tube.

A feature observed in the lattice Boltzmann model that cannot be eliminated through shock tube geometry is a gradual linear decline in the post-shock signal. A similar feature is observed in the data that NPL obtained during preliminary investigations using a shock tube at the UK's Cranfield University, described in Section 5, and has also been reported in measurements of side-wall post-shock pressure [28]. The model can also simulate ideal flow within the shock tube. The model records both pressure and temperature variation along the tube, and can be useful in identifying the sources of events and reflections observed in the data from the end wall (Figure 1).

2.3. Drop-weight systems for primary calibration

Two NMIs, MIKES and PTB, are developing drop-weight systems as new primary measurement standards for dynamic pressure calibrations. The drop-weight system is a simple and effective technique for calibrating high-amplitude dynamic pressure sensors. A free-falling mass falls along a guide system, strikes a piston at the top of a cylinder/chamber full of fluid, thus compressing the fluid. The increase in pressure

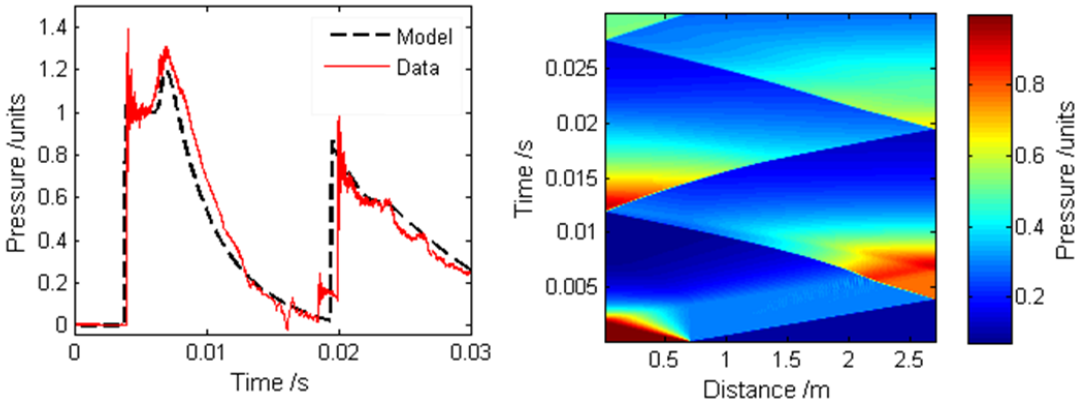

Figure 1. Left: Measured output data from the end wall (solid line) compared to an ideal flow from a lattice Boltzmann model (dashed line). Right: Predicted pressure variation with time, along the length of the tube, illustrates the source of peaks and reflections observed in the end wall signal.

acts on the sensor via the compressed hydraulic fluid. The pressure signal generated resembles a positive half-sine or squared sine wave [29, 30]. The magnitude and duration of the pressure pulse can be varied by using different masses released from different heights.

Figure 2 depicts two drop-weight pressure pulses of approximately 100 MPa and 400 MPa, respectively, measured for the MIKES drop-weight system. The maximum pressure is estimated from accelerometer measurements. With maximum values of the order of hundreds of MPa, drop-weight systems have much higher pressure capacities than shock tubes. However, the expected rise times for drop-weight systems are of the order of 1 to 2 ms leading to much reduced calibration bandwidths (less than 1 kHz) in comparison to shock tubes. Figure 3 shows a comparison of the expected frequency content of signals from a shock tube and a drop-weight system.

The systems being developed at the two NMIs are mechanically similar, and work over similar pressure intervals: the MIKES system from 100 MPa to 500 MPa, and the PTB system from 5 MPa to 500 MPa. Traceability for the MIKES system will be provided by calculating the acceleration of the piston from a traceable interferometric measurement of the mass displacement, and independent measurements of the mass of the drop-weight and the cross-section area of the piston. An equation for the pressure inside the chamber can then be derived from Newton's second law. The system developed at PTB is equipped with a laser for measuring the time variation of the pressure-dependent refractive index of the fluid under compression [32].

The drop-weight systems at both NMIs are still under development and as such there remains a lack of accurate knowledge of the form of the true pressure input. The analysis described in the remainder of the paper is therefore focused on the shock tube

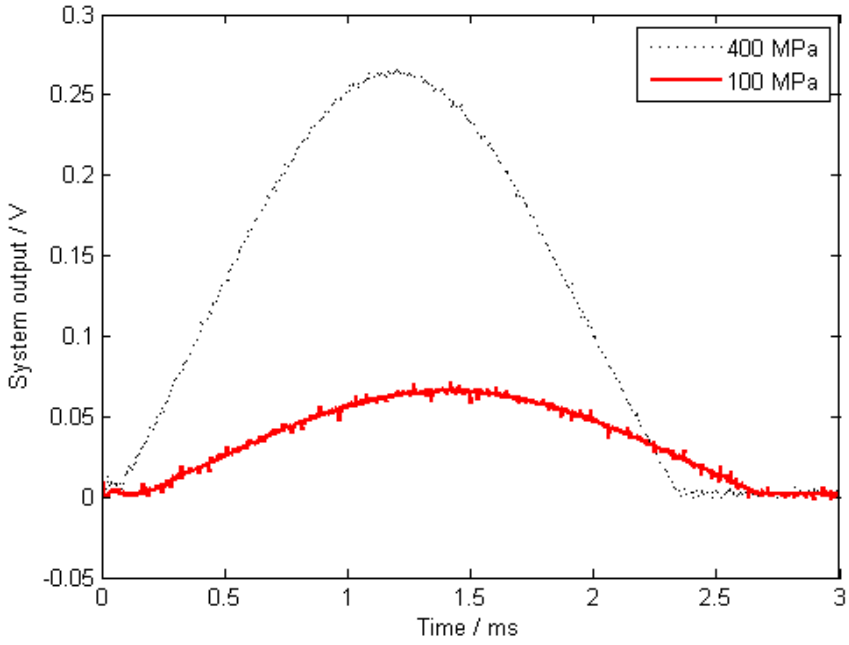

Figure 2. First measured output data from the MIKES drop-weight system.

system.

3. Simulation-based analysis

Simulation software has been developed in Matlab® [33] that predicts the frequency response of a measuring system with the shock tube, at a discrete set of frequency values. The software has been written such that when real measured data are available, the software can be used as a calibration tool, producing the uncertainties associated with the system response. Here we also consider the extension to system identification of a parametric model (see Section 4), allowing the response to be calculated over a continuous frequency interval.

3.1. Generating pressure input

Based on shock tube theory and the results from the modelling work described in Section 2.2, the pressure input for the shock tube is modelled as a fast-rising step (of the order of 0.1 μs) with the post-step amplitude determined from the starting pressure and temperature, and the shock speed.

3.2. Simulating the measuring system

A model for the measuring system was derived as follows. Based on the data sheets and user manuals for piezo-electric pressure sensors and charge amplifier units to be

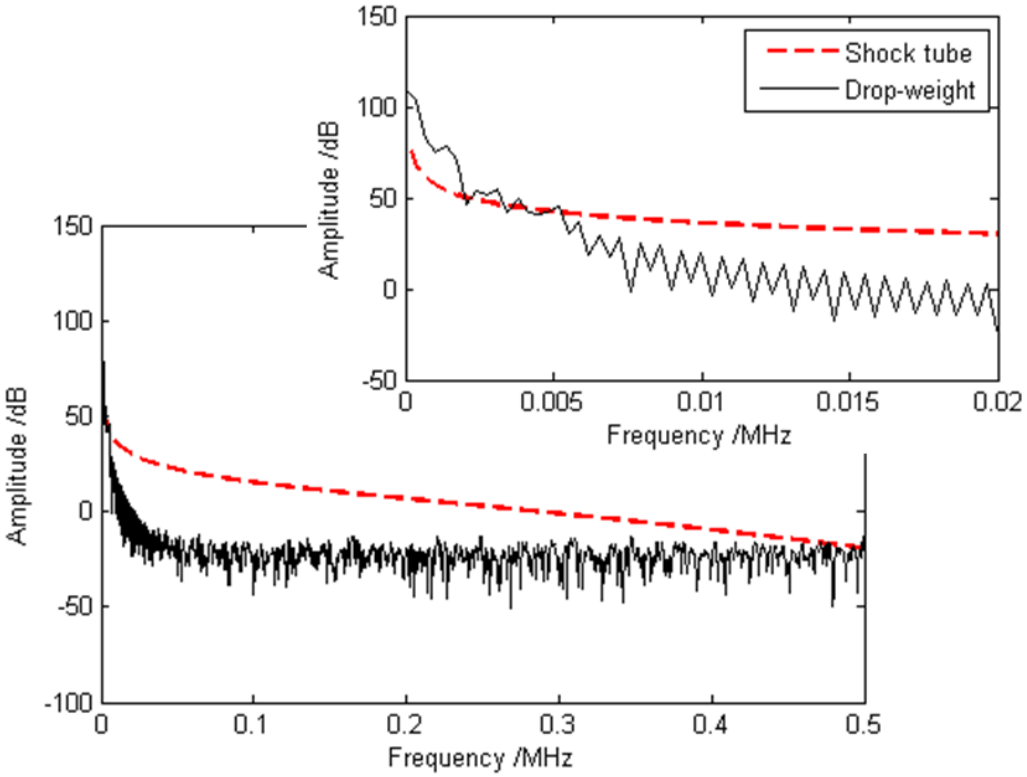

Figure 3. Frequency content of typical pressure signals generated by the shock tube and drop-weight systems. Gans-Nahman windowing technique [31] is applied to the signal generated by the shock tube. The smaller figure shows the two spectra in the low-frequency region.

used, an initial attempt to provide a parametric model for the system response includes a simple second order system, representing the pressure sensor, followed by a low-pass filter (LPF) to model the amplifier. The response of the sensor is described by the transfer function in the Laplace domain

$$H_S(S_0, \delta, \omega_0; s) = \frac{S_0 \omega_0^2}{s^2 + 2\delta\omega_0 s + \omega_0^2}, \tag{3}$$

for resonance frequency $\omega_0 = 2\pi f_0$, damping ratio δ and gain S_0. The charge amplifier, modelled by a 6th order Butterworth LPF, has transfer function

$$H_A(f_c; s) = \frac{b_0 s^6 + b_1 s^5 + \ldots + b_6}{a_0 s^6 + a_1 s^5 + \ldots + a_6},$$

where the coefficients a_i and b_i depend on the filter's cut-off frequency f_c. The transfer function describing the complete measuring system is then obtained as the cascade of the sensor and amplifier responses, which equals the product of the responses

$$H_{\text{model}}(S_0, \delta, \omega_0, f_c; s) = H_S(S_0, \delta, \omega_0; s) H_A(f_c; s)\,. \tag{4}$$

The parameters, $\boldsymbol{\phi}$, describing the model are therefore the damping ratio, gain and resonance frequency in expression (3), and the cut-off frequency of the LPF.

An output signal may then be simulated as the response of the system model (4) to a simulated input pressure signal, as described in Section 3.1.

3.3. System frequency response

To simulate the calibration as a simple deconvolution process, the sensor and charge amplifier are considered as a combined measuring system to be calibrated. Where the amplifier has previously been calibrated (i.e., the frequency response H_A has been obtained independently), a pre-processing deconvolution step may be applied to the data to correct for the effects of the amplifier.

Denote by $\boldsymbol{y}$ and $\boldsymbol{x}$, respectively, the time-varying values of the measured output signal and pressure input signal. From Equation (1), the system frequency response is calculated as the ratio of the Fourier transforms of the output signal $\boldsymbol{y}$ and assumed pressure input signal $\boldsymbol{x}$. Uncertainties associated with the pressure input and the sensor output are propagated through to the derived frequency response using a Monte Carlo method.

An uncertainty is associated with the initial pressure and temperature in the driven section of the shock tube, the speed of the shock front and its arrival time at the end wall, and the rise-time of the reflected shock. These parameters are varied to produce a different assumed input pressure signal for each Monte Carlo trial, assuming a clean step input, with amplitude calculated using Equation (2).

Prior to applying the Fourier transform, both the input and output signals are windowed using the Gans-Nahmann technique [31], further described in the Appendix. A discrete Fourier transform cannot be applied directly to a step-like signal, and a window is applied to the step to generate a signal with equal end-points. For an ideal step signal, where a constant post-step value has been reached, the choice of where to truncate the signal (i.e., where to apply the window) has a negligible effect on the resulting transform. When there is variation on the post-step signal, the choice of truncation point may affect the transform and should therefore be considered as a source of uncertainty. Therefore, uncertainties associated with the signal processing are considered by varying the truncation point of the output signal (implemented as a sliding window to maintain a constant signal length). Finally, measurement noise $\varepsilon(t)$ is added to the simulated output signal.

As an example, using the distributions listed in Table 1, Figure 4 shows the estimated amplitude and phase of the system frequency response, with associated standard uncertainties shown for each frequency. The reference values used to simulate the system response were chosen to be broadly indicative of those expected for the system used in the Cranfield tests, with the exception of the cut-off frequency. A relatively high cut-off frequency of 0.8 MHz was used to simulate the LPF response, to allow the behaviour around the resonance frequency to be clearly observable. The

Parameter	**Unit**	**Distribution/ Reference value**
Rise-time	ns	$\mathrm{N}(50,\, 20^2)$
Initial pressure	kPa	$\mathrm{N}(100,\, 0.5^2)$
Initial temperature	K	$\mathrm{N}(294,\, 0.1^2)$
Shock speed	$\mathrm{m\,s^{-1}}$	$\mathrm{N}(600,\, 2.5^2)$
End-wall arrival	ms	$\mathrm{N}(4,\, (1 \times 10^{-6})^2)$
Cut-off	ms	$\mathrm{R}(4.95,\, 5)$
Noise	V	$\mathrm{N}(0,\, 0.001^2)$
Resonance freq.	MHz	0.4
Cut-off freq.	MHz	0.8
Gain	-	1
Damping	-	0.1

Table 1. Parameters varied for assumed pressure input for simulations of measuring system calibration in a shock tube system, and reference values used for the simulated system response, where $\mathrm{N}(\mu,\, \sigma^2)$ describes a normal distribution with expectation μ and standard deviation σ, and $\mathrm{R}(a,\, b)$ describes a rectangular distribution with lower bound a and upper bound b .

amplitude estimates show good agreement with the simulated reference values up to the high-frequency points. The phase estimates deviate from the reference values around the resonance frequency at 0.4 MHz, but remain within the uncertainties. The relative uncertainty for amplitude is 1.5 % at the DC level and approximately 8.5 % around the resonance frequency at 0.4 MHz.

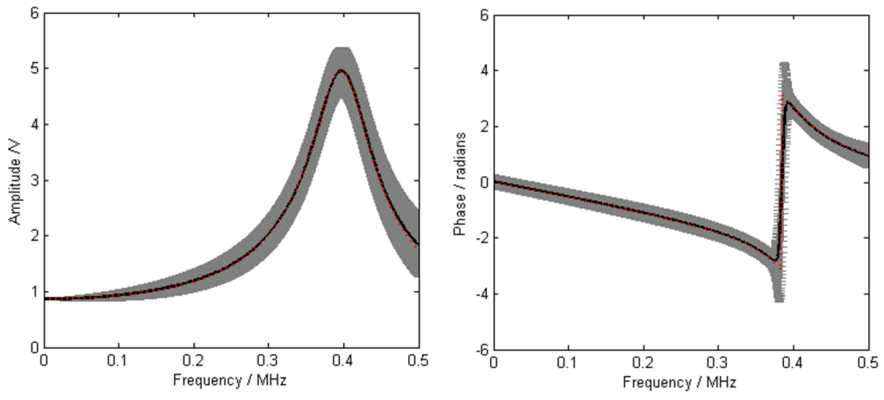

Figure 4. Mean amplitude (left) and phase (right) of system frequency response for a shock tube system from 100 000 Monte Carlo trials with assumed pressure input rise-time, step height, step time and signal cut-off varying as in Table 1. Error bars show standard deviation for each frequency. Red dashed line shows simulated reference response.

4. System identification

The frequency response calculated in Section 3.3 provides estimates (and associated uncertainties) of the amplitude and phase of the measuring system response at the given, discrete set of frequency values only. The frequencies at which the response is estimated are determined by the duration of the input pressure signal and the sampling frequency of the measuring system. Determining a parametric model to describe the system allows the response to be calculated on a continuous frequency interval and enables validation of sensor calibrations across different bandwidths. Depending on the particular parameterisation, it may also be possible to assign physical meaning to estimated parameters.

Assume that the statistical model for the data in the frequency domain is given in the form of real and imaginary parts:

$$\begin{aligned} \Re H(\omega_i) &= \Re H_{\text{model}}(\boldsymbol{\phi};\omega_i) + \varepsilon_i, \qquad i = 1,\dots,N\,, \\ \Im H(\omega_i) &= \Im H_{\text{model}}(\boldsymbol{\phi};\omega_i) + \varepsilon_{N+i}, \qquad i = 1,\dots,N\,, \end{aligned} \tag{5}$$

with errors $\varepsilon_i \sim \mathrm{N}(0,\sigma^2)$, where σ is assumed to be unknown, and substituting $s = j\omega$ in Equation (4). Here we use an input signal of 5 ms duration, sampled at 10 MHz, resulting in $N = 25\,000$ frequency points. We initially assume independence between frequencies to limit the required computational power. The use of a compact covariance matrix representation will be explored in the next stages of this project, to allow for consideration of correlation between frequencies. In future applications of this method, the unknown error parameter σ may be updated from experimentally determined measurement uncertainties.

For a given pressure input signal, $\boldsymbol{x}_{\Delta p}$, the measuring system model parameters $\boldsymbol{\phi}$ are then determined as

$$\hat{\boldsymbol{\phi}} = \arg\min_{\boldsymbol{\phi}}\{S(\boldsymbol{\phi})\},$$

with

$$\begin{aligned} S(\boldsymbol{\phi}) = \sum_{i=1}^{N} \big[&\left(\Re H_{\text{meas}}(\boldsymbol{y},\boldsymbol{x}_{\Delta p};\omega_i) - \Re H_{\text{model}}(\boldsymbol{\phi};\omega_i)\right)^2 \\ &+ \left(\Im H_{\text{meas}}(\boldsymbol{y},\boldsymbol{x}_{\Delta p};\omega_i) - \Im H_{\text{model}}(\boldsymbol{\phi};\omega_i)\right)^2 \big]\,, \end{aligned} \tag{6}$$

where the measured system response H_{meas} is the ratio of the (discrete) Fourier transforms of the output signal $\boldsymbol{y}$ and the pressure input signal $\boldsymbol{x}_{\Delta p}$. Calculation of $\hat{\boldsymbol{\phi}}$ is carried out using nonlinear least squares with the Levenberg-Marquardt algorithm [34]. Uncertainties associated with the estimated model parameters, assuming the statistical measurement model (5), are calculated as

$$\boldsymbol{U}_{\hat{\phi}} = (\boldsymbol{J}_{\hat{\phi}}{}^{\top}\boldsymbol{J}_{\hat{\phi}})^{-1}\frac{S(\hat{\boldsymbol{\phi}})}{N-4}\,, \tag{7}$$

where $\boldsymbol{J}_{\hat{\phi}}$ denotes the Jacobian of expression (6) with respect to $\boldsymbol{\phi}$ evaluated at $\hat{\boldsymbol{\phi}}$, and $N-4$ denotes the degrees of freedom.

Applying the system identification to a simulated shock tube output signal, with the known reference pressure step input assumed, recovers good estimates of the parameters describing damping, gain and resonance frequency of the system. Table 2 gives the reference values of the parameters used to simulate the measurement along with the estimates and relative uncertainties, using expressions (6) and (7) respectively. Note that a relatively low value of 0.6 MHz was used for the LPF cut-off frequency. A value close to the resonance behaviour was chosen to test the ability of the algorithm to identify the resonance frequency when a relatively low-frequency filter is applied.

Parameter	**Damping**	**Gain**	**Res. freq.**	**Cut-off freq.**
Unit	-	-	MHz	MHz
Reference value	0.1	1	0.4	0.6
Estimate using reference input	0.0999	0.9990	0.4001	0.5999
Relative uncertainty (%)	0.009	0.003	0.001	0.003
Mean	0.1001	1.0012	0.4002	0.5999
Standard deviation	0.0001	0.0171	0.0001	0.0002

Table 2. Mean parameter values, and standard deviations, from 5000 Monte Carlo trials, with assumed pressure input varying according to the distributions given in Table 1. The reference parameter values are those used to simulate the measured data. Also shown are the estimates and relative uncertainties (7) returned by the optimisation (6) when the reference pressure input is used.

The sensitivity of the estimated system parameters to the assumed pressure input is investigated using a Monte Carlo method. Here, the variables determining the generated pressure are varied, according to the distributions listed in Table 1, to produce a different assumed input for each trial, and measurement noise $\varepsilon(t)$ is added to the simulated output signal. The end-wall arrival time is assumed to be known exactly for the system identification, as the initial response time of the system cannot be controlled by the four parameters considered in model (4). Subsequent system models may incorporate a delay parameter, whose estimate would depend on the shock arrival time and associated uncertainty.

The last two lines of Table 2 list the mean value for each parameter obtained by a Monte Carlo method, along with their standard deviations. All four parameters are identified well and the modelled output, generated using the reference pressure input and estimated system parameters in Table 2, provides a good fit to the simulated reference output (Figure 5). Plotting the results from each Monte Carlo trial gives a clearer indication of which effects on the input pressure signal have an appreciable influence on the estimates of the model parameters, and helps to identify correlations between the fitted parameters. Therefore, we carried out a further, comprehensive simulation study using different values for the initial pressure and input signal rise-time. Within the regions studied, the variation in the assumed initial pressure has the most significant influence, with the step rise-time having a lesser, but also observable, effect.

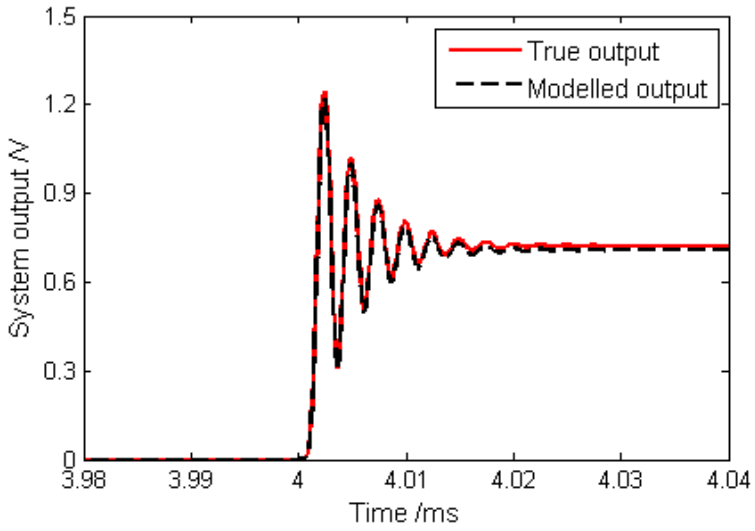

Figure 5. System output for the reference parameter values (dashed black line) and estimated parameter values (solid red line) from the system identification with uncertainties associated with the values of the input pressure signal.

For example, the influence of these two input variables on the fitted gain parameter can be seen in Figure 6(a). As the value of the assumed initial pressure decreases, the value of the fitted gain has to be increased to fit the model to the measured signal. For a constant initial pressure, there is also a small increase in fitted gain as the rise-time of the pressure step increases. For starting pressures below approximately 0.05 MPa, the fitted gain value becomes fixed at the upper boundary given in the optimisation function, and the fitted damping parameter is reduced to compensate (Figure 6(b)). While there will clearly be correlations between the fitted system parameters, these correlations are not considered in the values given in Table 2.

5. Shock tube data

In this Section, we briefly describe the application of the system identification techniques described in Section 4 to measured data available from shock tube firings. These data are from early measurements from the SP shock tube and the preliminary work carried out at Cranfield University.

The Cranfield shock tube has a driven section of length 7.3 m and diameter 81.3 mm. Measured data was analysed from six different firings of the Cranfield shock tube, with aluminium diaphragms and with the same piezo-electric sensor and charge amplifier used each time. Burst pressures varied from 6.9 MPa to 8.3 MPa, giving initial pressure ratios of approximately 70 – 80. The data showed variations in the step height, presumably due to different burst pressures, and also differences in a gradual linear trend observed in the post-step section of the output signal. A consistent feature seen in all data sets is a series of impulse-like disturbances, decreasing in size, in the post-step section of the

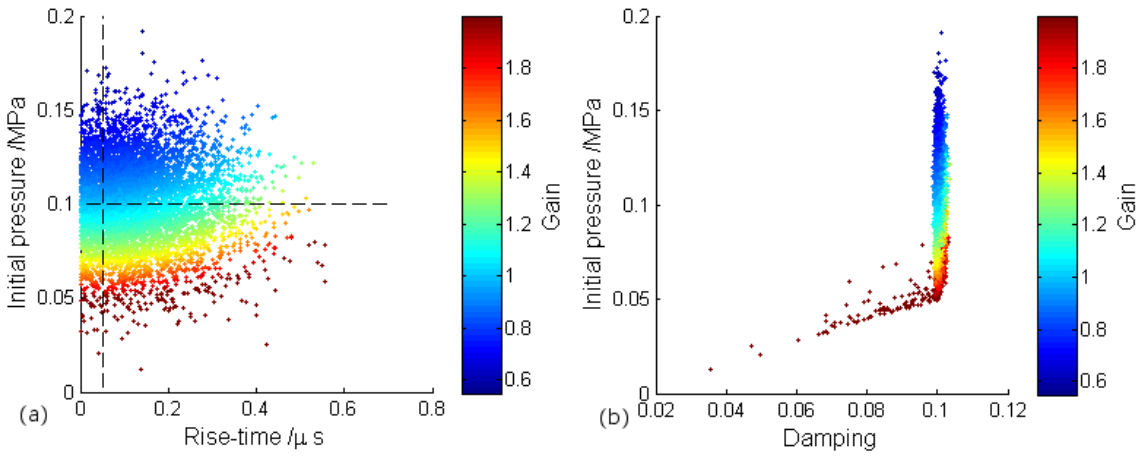

Figure 6. Fitted values for the system gain (shown as colour) with varying assumed initial pressure and (a) step rise-time, (b) fitted system damping. Note that for each data point shown, initial temperature and shock speed also vary. Dashed lines in (a) show the reference values of both parameters.

output signal.

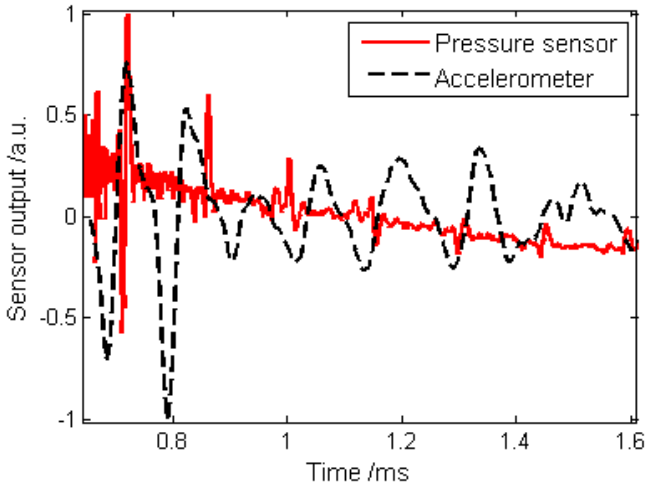

Figure 7. Data (shifted and scaled) from the accelerometer and end-wall sensor in a typical run.

Modern dynamic pressure sensors are designed to be reasonably insensitive to accelerations. The sensor used in the Cranfield shock tube uses a seismic mass to compensate for sensitivity to acceleration. This mechanism is not explicitly included in the sensor response model (3), but could be incorporated as a coupled, damped oscillator. However, comparisons of output signal with vibrations measured by an accelerometer fitted within the side-wall of the shock tube (Figure 7), suggest that the peaks observed in the measuring system output may be, at least partially, due to

vibrations during the shock tube firing that the compensation mechanism of the sensor is not able to deal with adequately. The same sensor has since been used in a prototype shock tube recently installed at NPL. The acceleration-compensation has been tested by firing the shock tube with the sensor mounted on the end-wall, but completely sealed off from the gas in the tube, therefore experiencing no pressure change. Relatively large amplitude events recorded by the measuring system support the suggestion that the vibrations produced by firing a shock tube are of a greater amplitude and/or frequency than the sensor compensation mechanism can correct for. For the system identification described in Section 5.1, the post-shock data was truncated before the arrival of the first of these larger disturbances.

Three data sets from the SP shock tube are considered. The SP shock tube has driven length 2 m, diameter 0.1 m and uses layered cellophane diaphragms. Typical burst pressures are 0.6 MPa. Again, a piezo-electric sensor and charge amplifier make up the measuring system, though both are different from those used for the Cranfield measurements.

5.1. System identification

A clean step pressure input is assumed in all cases, with a rise-time of 50 ns. The step amplitude ΔP is determined from initial pressure and shock speed estimates, using Equation (2).

Data sheets for the sensor and amplifier used in the Cranfield shock tube give values of 0.4 MHz and 0.2 MHz for the natural frequency of the sensor and the cut-off frequency of the analog low-pass filter of the charge amplifier, respectively. These values can be employed to justify the determined model parameters.

Figure 8 shows the identified parameter values for the six firings of the Cranfield shock tube. At this stage it is assumed that the pressure input is known exactly, i.e., no uncertainties are associated with its parameters. The error bars on the parameter values represent the uncertainties (7) under the assumption of the measurement model (5).

With the exception of the second firing, the two frequency parameters show a consistent fitted value across the data sets. The cut-off frequency corresponds to that expected from the manufacturer's data sheet, while the resonance frequency is slightly lower than that expected from the sensor documentation. However, given that the stated frequency of 0.4 MHz is greater than the cut-off frequency of the LPF, it is very likely that much of the activity closer to the resonance has been lost, therefore making it difficult to fit this parameter. Future measurements using the NPL shock tube will use an amplifier setting that does not suppress the sensor's resonance frequency. The damping parameter δ is consistent across the six runs, but with larger uncertainties appears to be harder to fit than the frequency parameters. A less consistent fit is seen for the gain parameter S_0. However, this parameter is very sensitive to the estimated value of the pressure height. With a more accurate knowledge of this value, or analysis that took into account the uncertainty of the value, consistency across the runs may

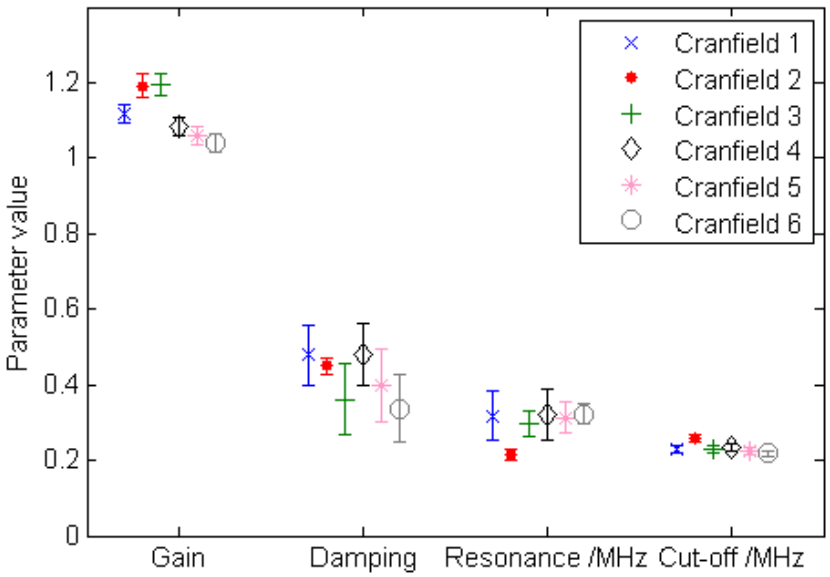

Figure 8. Identified values for system parameters, assuming ideal step input. The error bars on the parameter values represent the standard uncertainties (7) calculated under the assumption of the measurement model (5).

improve.

Figure 9 shows the measured frequency response for a single run from the Cranfield shock tube, compared to the fitted frequency response model, assuming an ideal step input. While the model reproduces the general shape of the measured response, much of the finer structure is not captured. These differences indicate that either the system model (4), or the measurement model (5), or both, are not yet fully adequate.

The model is also tested by simulating an output signal in the time domain, based on the assumed pressure input and modelled system response (Figure 9). Again, although the rise and over-shoot of the signal are captured well, the later disturbances in the signal are not explained by the current model (4).

As the current model cannot fit the post-shock disturbances after approximately 0.65 ms, the system identification is repeated using only the signal up to 0.65 ms. Figures 10 and 11 show the optimised parameter values, and the fitted model for a single run, respectively.

The parameter values remain largely similar to those shown in Figure 8, which may be expected given that the initial system identification fitted just this first part of the post-shock signal. The notable differences are the damping parameters, which have smaller uncertainties but are not consistent across the runs, and the consistency now observed across the resonance values, which also have smaller uncertainties. The frequency response in Figure 11 illustrates that the resonance frequency is now more easily identifiable, without the noise from the omitted post-shock oscillations.

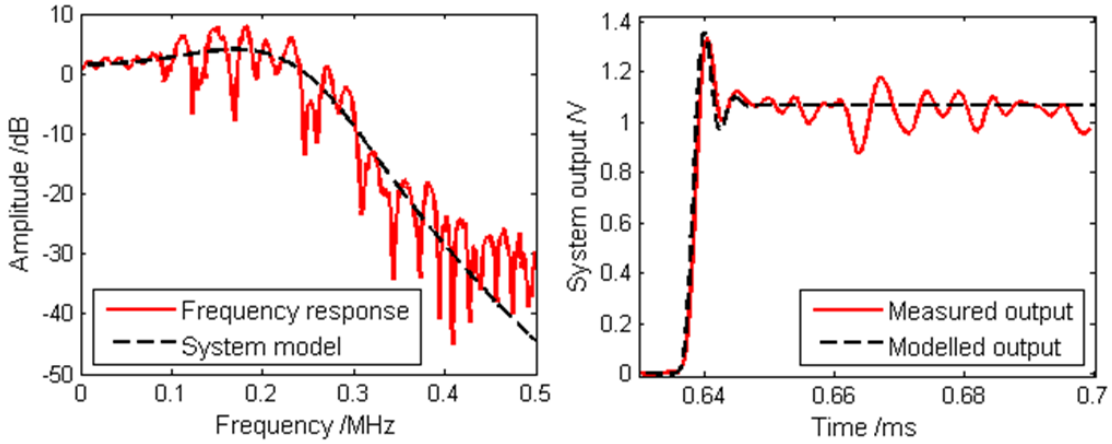

Figure 9. Left: Fitted frequency response for single run from Cranfield shock tube. Right: Model validation of system output for single run from Cranfield shock tube.

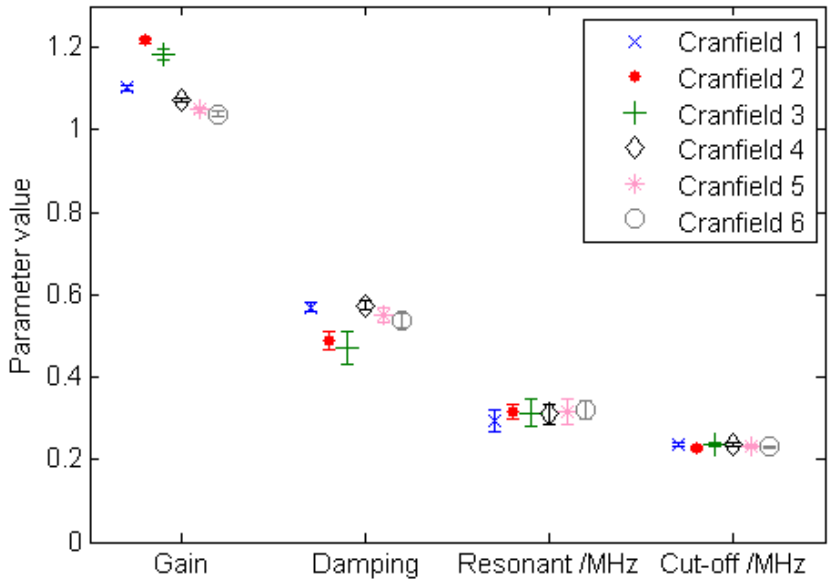

Figure 10. As for Figure 8, using measured output signals up to 0.65 ms.

Figure 12 shows a single output signal from the SP shock tube, and the frequency response of the system, assuming a clean step pressure input. There is a more obvious peak frequency than in the Cranfield data (see Figure 9), clear both in the time and frequency domain. The natural frequency of the sensor is quoted as 0.16 MHz, within the peak frequency range seen in Figure 12. A sharp drop-off follows this peak, but subsequently there is less evident attenuation at the higher frequencies than seen in the Cranfield data, implying that any cut-off occurs beyond the natural frequency of the

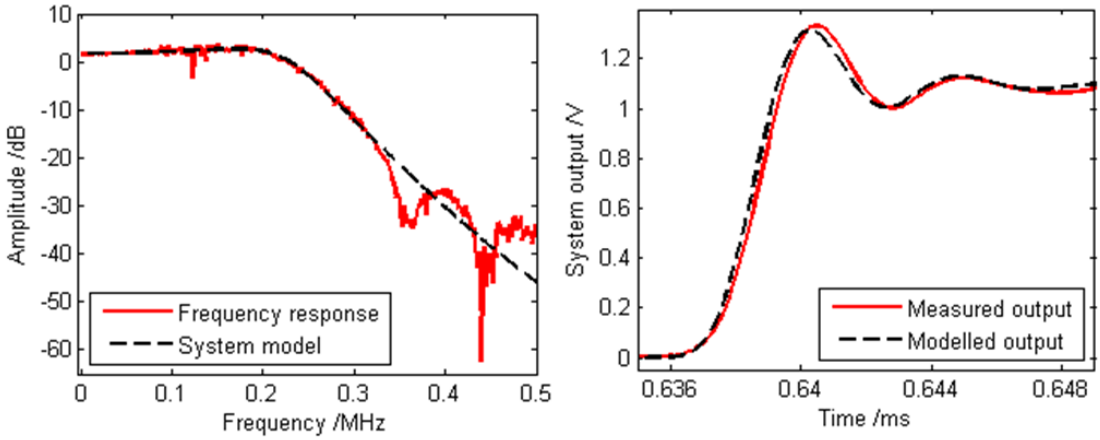

Figure 11. As for Figure 9, using a measured output signal up to 0.65 ms

sensor. For the system identification, the influence of the amplifier on the frequency response was assumed to be negligible.

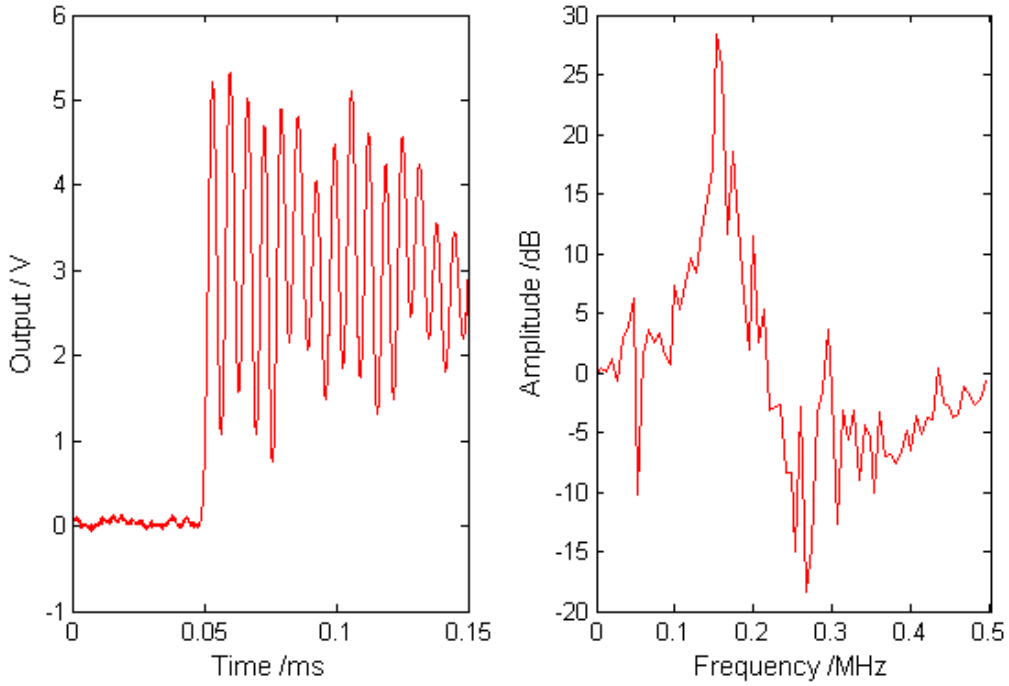

Figure 12. Output signal from measuring system in the SP shock tube (left), and derived frequency response for the system (right), assuming a clean step input.

In the optimisation process, the estimated sensor frequency corresponds to that given by the manufacturer's data sheet, and is consistent across the three measurement

runs (Figure 13). The damping estimate is also consistent across the three, and significantly less than that derived for the Cranfield system. The lack of damping is evident in Figure 12, with little attenuation of the post-shock ringing. As before, the gain parameter is more varied across the three runs, but again is significantly affected by the assumed height of the step input. Gain estimates will therefore be improved through more accurate measurements of the starting pressures and shock speed for each firing.

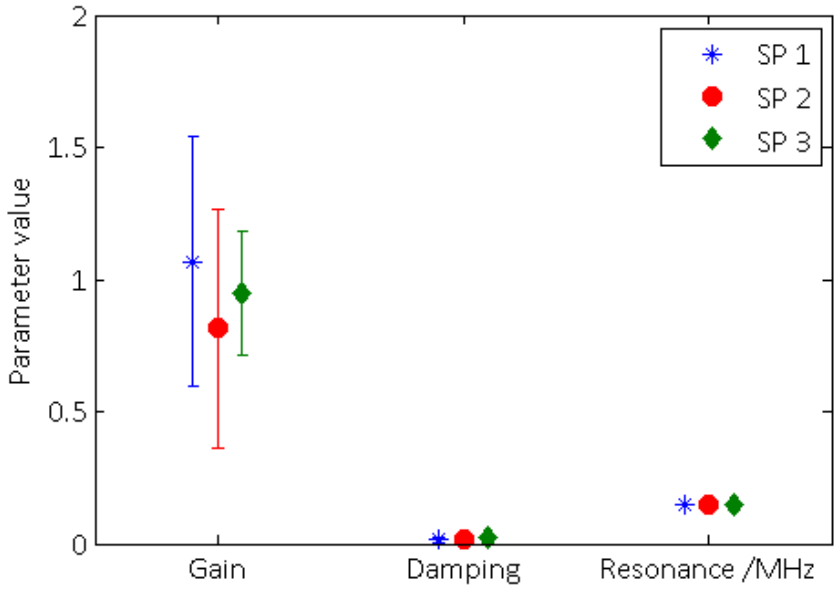

Figure 13. Identified values for system parameters in the SP shock tube, assuming a clean step input and no LPF in the system model (4). Error bars represent standard uncertainties (7) assuming the measurement model (5).

The fitted model is shown with the measured data both in the frequency and time domain in Figure 14. The model captures the system response much more fully than in the case of the Cranfield data, though still fails to capture some features.

Although the parametric model identified for the system is reasonably consistent across multiple data sets, and for two different shock tubes, Figures 9 and 14 show that there are many features within the data that are not explained by the model. System identification assumes knowledge of the input signal to the system and for the current problem we have to rely on a model for this input. The consistency of parameters for the system model may imply that it is the pressure input model that is too simple. However, empirical results also suggest that some features in the post-shock signal may be due to acceleration compensation in the sensor. An extension of the simple sensor model (3) to account for such a coupled system may improve the fit to observed data, and will be investigated in future work. Further experiments are being carried out to validate the pressure input model and to investigate extension of the system and the

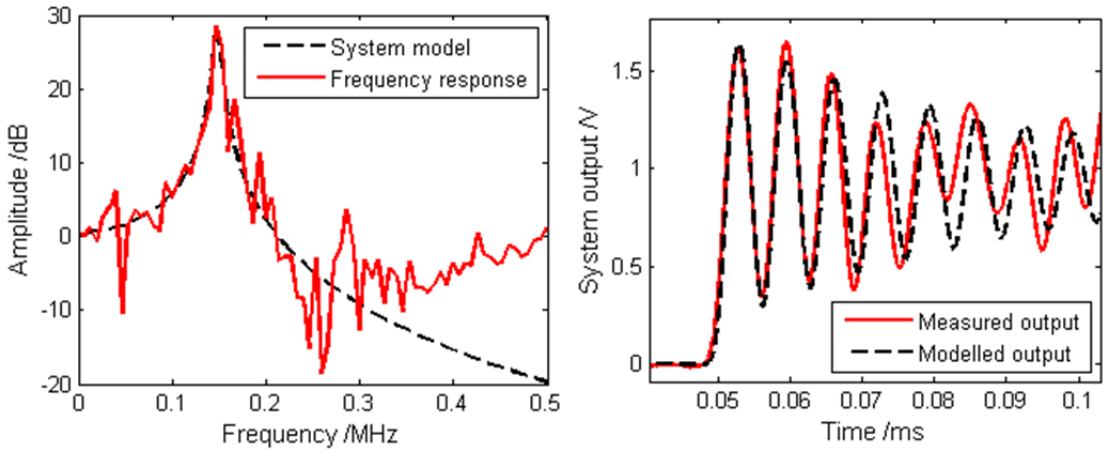

Figure 14. Left: Fitted model and measured frequency response, assuming a step pressure input, for a firing of the SP shock tube. Right: Measured output from the SP shock tube and modelled output derived from fitted system parameters, assuming a step input.

measurement models.

6. Conclusions

The development of primary standard calibration systems for dynamic pressure presents a number of mathematical and metrological challenges. The current EMRP project focuses on the use of shock tubes and drop-weight systems to generate wide-bandwidth time-varying pressure signals and here we introduced some of the specific issues that arise with these systems, and our approaches to tackling them.

Shock tubes can generate repeatable fast-rising step-like signals. However, a significant challenge in using these signals for calibration purposes is the inability to independently measure the pressure change. To this end, we assumed a step-like input with height and rise-time determined from measurements of shock speed and initial pressure. Using a comprehensive simulation study we demonstrated that knowledge of the initial pressure has a strong impact on the estimation result. Our system identification fits a consistent model across multiple firings of the tube, but our current model does not explain all features observed in the data. The next stages of our work will attempt to identify the sources of these features, and in particular whether they are generated within the shock tube itself or the sensor. A prototype shock tube developed at NPL is currently being used to try to identify and quantify any sources of non-ideal behaviour within the shock tube. The repeatability observed over multiple firings of this shock tube with diaphragms of different material, suggest that many of the post-shock features of the measured signal may be a sensor response. A comparison of different sensors across the NPL and SP shock tubes will also help to distinguish between aspects

of shock tube and sensor behaviour. Disturbances generated by the shock tube can to some extent be minimised or eliminated through shock tube design. Components of the output that are inherent in the sensor response must be incorporated into our sensor model. A potential extension to the representation of the sensor may be to consider a coupled system, to better model vibrations or reflections within the sensor itself.

For the drop-weight system different methods to obtain an independent measurement of the input pressure signal are possible. Each of these methods incorporate measurements or characteristics of fluid properties that are not yet fully investigated in terms of mathematical models. To this end, future research at MIKES and PTB will be carried out to derive a suitable model that can be applied in a system identification to generate input pressure signals from traceable measurement of certain parameters similar to the shock tube approach.

The final aim is to use a comparison between the different drop-weight and shock tube systems as a validation tool for the system identification approach developed. Where the calibration process has fitted a parameterised model of the measuring system, comparison across the calibration systems will be straightforward. The ability to compare frequency responses calculated from the different calibration systems will depend on the extent of overlap between the respective frequency intervals, in terms of meaningful data for amplitude and phase at those frequencies. With a fully developed model for drop-weight pressure, simulations may be used to determine to what extent such a comparison may be possible in practice, before final development of the standard systems.

Acknowledgments

This work was funded through the European Metrology Research Programme (EMRP) Project IND09 Dynamic. The EMRP is jointly funded by the EMRP participating countries within EURAMET and the European Union.

Valuable support has been provided by project partners: Stephen Downes (NPL), Ian Robinson (NPL), Sari Saxholm (MIKES), Holger Schönekeß (PTB), and Martin Zelan (SP). Experimental work has been supported by Kistler.

The authors wish to thank the two referees for valuable comments and suggestions for improving this paper.

Appendix

Applying a discrete Fourier transform (DFT) directly to a step function results in errors as the DFT for finite intervals is exact only for band-limited signals that have a smooth periodic extension [35]. The reason is that taking the DFT of a signal on a finite interval implies the approximation of the Fourier series of its infinite periodic extension. When the signal values at the interval end points are unequal this periodic extension has discontinuities. For an increasing sampling frequency the Fourier series of the periodic

extension at the end points of the original interval then converges to the average of both values resulting in significant errors, see Theorem 2.4 in [35]. In addition, the unequal values at the end points result in the so called Gibbs effect - a ringing in the inverse DFT [35]. To this end, various techniques have been applied to the spectral analysis of step-like functions. These techniques generally require the addition, subtraction or multiplication of an additional signal with the original to create a signal that is zero-valued at its end-points. An alternative approach is to differentiate the step response to obtain an impulse response signal. The disadvantage with this approach is the increase in uncertainties caused by differentiating the signal.

The approach adopted here was described by Gans and Nahman [31]. Their technique involves the extension of the original, truncated step-like time series $v(t)$ as follows. Assume the original, step-like signal $v(t)$ is measured for $t \in [0, T]$ and satisfies

$$\begin{aligned} v(t) &= 0, \qquad \text{for } t < 0, \\ v(t) &= v(T), \quad \text{for } t > T, \end{aligned}$$

implying that the signal has reached a final, steady value when it is truncated at $t = T$. Then a new function $g(t)$ is defined on the interval $[0, 2T]$ as

$$g(t) = v(t) - v(t - T),$$

which then satisfies $g(0) = g(2T) = 0$, hence it is a signal with zero-valued end points. This technique effectively doubles the length of the time signal and number of samples. It therefore doubles the number of harmonic frequencies at which the FFT is defined. However, the FFT solution is zero at the even harmonics [31].

References

[1] BIPM, IEC, IFCC, ISO, IUPAC, IUPAP, and OIML. *Evaluation of Measurement Data - Guide to the Expression of Uncertainty in Measurement*. Joint Committee for Guides in Metrology, Bureau International des Poids et Mesures, JCGM 100, 2008.

[2] BIPM, IEC, IFCC, ISO, IUPAC, IUPAP, and OIML. *Evaluation of Measurement Data - Supplement 1 to the 'Guide to the Expression of Uncertainty in Measurement' - Propagation of Distributions Using a Monte Carlo Method*. Joint Committee for Guides in Metrology, Bureau International des Poids et Mesures, JCGM 101, 2008.

[3] BIPM, IEC, IFCC, ISO, IUPAC, IUPAP, and OIML. *Evaluation of Measurement Data - Supplement 2 to the 'Guide to the Expression of Uncertainty in Measurement' - Extension to any number of output quantities*. Joint Committee for Guides in Metrology, Bureau International des Poids et Mesures, JCGM 102, 2011.

[4] L. Ljung. *System Identification: Theory for the User*. Prentice Hall, 1998.

[5] R. Pintelon and J. Schoukens. *System Identification: A Frequency Domain Approach*. John Wiley & Sons, 2001.

[6] A. Link, A. Täubner, W. Wabinski, T. Bruns, and C. Elster. Modelling accelerometers for transient signals using calibration measurements upon sinusoidal excitation. *Measurement*, 40:928–935, 2007.

[7] C. Elster, A. Link, and T. Bruns. Analysis of dynamic measurements and determination of time-dependent measurement uncertainty using second-order models. *Measurement Science and Technology*, 18:3682–3687, 2007.

[8] S. Eichstädt. *Analysis of Dynamic Measurements - Evaluation of Dynamic Measurement Uncertainty*. PhD thesis, TU Berlin, PTB report IT-16 ISBN 978-3-86918-249-0S, 2012.

[9] T. J. Esward, C. Elster, and J. P. Hessling. Analysis of dynamic measurements: new challenges require new solutions. In *XIX IMEKO World Congress on Fundamental and Applied Metrology*, 2009.

[10] L. Klaus, T. Bruns, and M. Kobusch. Determination of Model Parameters for a Dynamic Torque Calibration Device. In *XX IMEKO World Congress, Busan, Republic of Korea*, 2012.

[11] M. Kobusch, L. Klaus, and T. Bruns. Model-Based Analysis of the Dynamic Behaviour of a 250 kN Shock Force Calibration Device. In *XX IMEKO World Congress, Busan, Republic of Korea*, 2012.

[12] C. Schlegel, G. Kiekenap, and R. Kumme. Application of a Scanning Vibrometer for the Periodic Calibration of Force Transducers. In *XX IMEKO World Congress, Busan, Republic of Korea*, 2012.

[13] C. Elster and A. Link. Uncertainty evaluation for dynamic measurements modelled by a linear time-invariant system. *Metrologia*, 45:464–473, 2008.

[14] S. Eichstädt, C. Elster, T. J. Esward, and J. P. Hessling. Deconvolution filters for the analysis of dynamic measurement processes: a tutorial. *Metrologia*, 47:522–533, 2010.

[15] S. Eichstädt, A. Link, P. Harris, and C. Elster. Efficient implementation of a monte carlo method for uncertainty evaluation in dynamic measurements. *Metrologia*, 49:401–410, 2012.

[16] A. V. Oppenheim and R. W. Schafer. *Discrete-Time Signal Processing*. Prentice Hall, 1989.

[17] J. Schoukens and R. Pintelon. *Identification of Linear Systems - A Practical Guideline to Accurate Modeling*. Pergamon Press, 1991.

[18] V.E. Bean, W.J. Bowers, W.S. Hurst, and G.J. Rosasco. Development of a primary standard for the measurement of dynamic pressure and temperature. *Metrologia*, 30:747–750, 1994.

[19] V.E. Bean. Dynamic pressure metrology. *Metrologia*, 30:737–741, 1994.

[20] A. G. Gaydon and I. R. Hurle. *The shock tube in high-temperature chemical physics*. Chapman & Hall, 1963.

[21] A. C. G. C. Diniz, A. B. S. Oliveira, J. N. S. Vianna, and F. J. R. Neves. Dynamic calibration methods for pressure sensors and development of standard devices for dynamic pressure. *XVIII IMEKO World Congress, Metrology for a Sustainable Development, 17-22 Sept. Brazil*, 2006.

[22] V. Stankevic and C. Simkevicius. Use of a shock tube in investigations of silicon micromachined piezoresistive pressure sensors. *Sens. Actuators*, 86:58–65, 2000.

[23] ISA-37.16.01-2002. *A Guide for the Dynamic Calibration of Pressure Transducers*. ISA, 2002.

[24] S. Downes, A. Knott, and I. Robinson. Towards a shock tube method for the dynamic calibration of pressure sensors. In *Hopkinson Centenary Conference, Cambridge: Special issue of the Philosophical Transactions of the Royal Society of London, Series A*, 2014.

[25] S. Succi. *The Lattice Boltzmann Equation: For Fluid Dynamics and Beyond*. Oxford University Press, 2001.

[26] C. Matthews, T. J. Esward, S. Downes, A. Knott, and I. Robinson. Lattice Boltzmann method applied to non-ideal diaphragm opening in shock tubes. *Submitted to Shock Waves*, 2013.

[27] P. Gaetani, A. Guardone, and G. Persico. Shock tube flows past partially opened diaphragms. *J. Fluid Mech.*, 602:267–286, 2008.

[28] D. F. Davidson andR. K. Hanson. Interpreting shock tube ignition data. In *WSSCI Fall Meeting, 20-21 Oct. University of California*, 2003.

[29] M. S. Nawrocka, W. J. Bock, and W. Urbanczyk. Dynamic pressure calibration of the fibre-optic sensor based on birefringent side-hole fibers. *IEEE Sensors Journal*, 5:1011–1018, 2005.

[30] F. Marian, P. Box, and A. McLean. *Dynamic Impulse Calibration of 100 MPa Blast Pressure Transducers*. Australian Government Department of Defence, Defence Science and Technology Organisation, Report no. DSTO-TN-052, 2003.

[31] W. L. Gans and N. S. Nahman. Nahman continuous and discrete Fourier transforms of steplike waveforms. *IEEE Trans. on Instr. and Meas.*, 31:2, 1982.

[32] T. Bruns, E. Franke, and M. Kobusch. Linking dynamic to static pressure by laser interferometry. *Metrologia*, 50:580–585, 2013.

[33] MATLAB R2013a. http://www.mathworks.co.uk/, 2013.

[34] D. W. Marquardt. An algorithm for least-squares estimation of nonlinear parameters. *Journal of the Society for Industrial and Applied Mathematics*, 11:431–441, 1963.

[35] W. L. Briggs and V. E. Henson. *The DFT: An Owner's Manual for the Discrete Fourier Transform.* Society for Industrial and Applied Mathematics, 1995.